Research Article

Pablo Muniz-Cánovas*, Yuri Barmenkov, Ámbar A. Reséndiz-Córdova, Vicente Aboites, José-Luis Cruz, and Miguel V. Andrés

The use of a supercontinuum light source for the characterization of passive fiber optic components

https://doi.org/10.1515/phys-2024-0092
received July 01, 2024; accepted August 29, 2024

Abstract: In this article, we report the application of a commercial supercontinuum light source for testing fiber optics components in a broad optical range. We demonstrate that this kind of light can be successfully used to measure the parameters of a number of passive fiber components, such as fiber Bragg gratings, fiber couplers, wavelength division multiplexers, and fibered isolators. We also show that near the double wavelength of the pulsed laser used to pump the nonlinear fiber generating the supercontinuum, the standard optical spectrum analyzers demonstrate the false spectral peak that affects the test results and that using a simple low-cost monochromator placed at the supercontinuum source output permits the elimination of this peak. The results of experiments related to the characterization of passive fiber devices in the broad optical range, from 1 μm to more than 2 μm, are discussed in detail as possible applications of the proposed technique.

Keywords: supercontinuum light, fiber optic devices, optical testing

*** Corresponding author: Pablo Muniz-Cánovas,** Centro de Investigaciones en Óptica, A.C., Loma del Bosque 115, 37150, León, Gto., Mexico, e-mail: pablomc01@gmail.com
Yuri Barmenkov: Centro de Investigaciones en Óptica, A.C., Loma del Bosque 115, 37150, León, Gto., Mexico, e-mail: yuri@cio.mx
Ámbar A. Reséndiz-Córdova: Departmento de Ingeniería Química, Universidad Tecnológica de México Campus León, Blvd. Juan Alonso de Torres Pte. 1041, 37200, León, Gto., Mexico, e-mail: marcelineoverland@gmail.com
Vicente Aboites: Instituto Euro-Americano, Alfredo Duges 28, 36271, Guanajuato, Gto., Mexico, e-mail: vicenteaboites@gmail.com
José-Luis Cruz: Departamento de Física Aplicada, Instituto de Ciencia de Materiales, Universidad de Valencia, 46100, Valencia, Spain, e-mail: jose.l.cruz@uv.es
Miguel V. Andrés: Departamento de Física Aplicada, Instituto de Ciencia de Materiales, Universidad de Valencia, 46100, Valencia, Spain, e-mail: miguel.andres@uv.es

1 Introduction

Supercontinuum is an optical phenomenon related to the dramatic broadening of the optical spectrum of short laser pulses used as the pump of a nonlinear optical medium. This phenomenon is achieved by a nonlinear process based mainly on the modification of the refractive index of the optical medium, which depends on the intensity of the pump pulses [1,2]. In solid materials, supercontinuum generation is achieved using ultrashort high-intensity laser pulses, typically on the femtosecond (10^{-15} s) or picosecond (10^{-12} s) scale, which induce strong molecular vibrations resulting in electronic, molecular, and vibrational distortions in the material [3]. Thus, the laser pulses experience a number of nonlinear effects, including self-focusing, various types of scattering, phase self-modulation, two- and four-wave mixing, and others, which cause a strong broadening of the pulse spectrum [4–7].

In the case of optical fibers, the relationship between the peak power of the pulses and the length of interaction with the material can be controlled more efficiently than in bulk materials. The pump pulse magnitude and energy can be significantly reduced if the fiber has a suitable waveguide structure. For instance, small-effective-mode fibers demonstrate strong energy conversion of relatively narrow-band pump pulses to broadband supercontinuum ones due to a significant increase in the pulses' intensities [8–11]. A similar effect is observed in fiber tapers, which are also used to generate supercontinuum, as they allow high nonlinear interaction over a relatively short fiber length [12,13]. Recently, grade-index multimode fibers were used as a nonlinear medium for broad-band supercontinuum generation [14].

Photonic crystal fibers (PCFs) contribute significantly to SC generation due to their specific geometrical structure, which results in unique optical properties. The microstructure shape of PCFs, typically featuring a hexagonal periodic structure of air holes running along the fiber length, allows for precise control over the fiber's dispersion and nonlinear

characteristics. When intense laser pulses travel along a PCF, the combined effects of nonlinear optical processes interact with the tailored dispersion properties of the fiber. This interaction causes the broadening of the spectrum of the injected light, resulting in the supercontinuum generation. The ability to engineer the dispersion profile of PCFs makes them ideal for efficiently producing supercontinuum light sources with desired spectral properties [15–17].

The SC light has enabled a wide range of applications, such as frequency clocks [18], broadband spectroscopy [19,20], phase control and stabilization [21], ultra-short pulse compression [22,23], fluorescence/stimulated emission depletion (STED) microscopy and imaging for chemical and biological sciences [24–27], STED lithography [28], optical coherence tomography [29–31], smart target recognition [32], microwave photonic [33], optical communications [34,35], spread spectrum LIDAR and atmospheric sciences [36–38], illumination control [39,40], pulse generation in the order of attoseconds (10^{-18} s) [41,42], and coherence control [43–45]. The application of supercontinuum light spanning from 450 to 1,650 nm for measuring the absorption spectrum of erbium-doped fiber and transmission spectra of a photonic bandgap fiber and a fiber cavity is discussed in the study by Narukawa *et al.* [46], whereas the use of the optical filter of the SC light, tunable in the range from 700 to 1,800 nm with 1.3 nm resolution, for the characterization of fiber optical components and systems was proposed in the study by Lehtonen *et al.* [47]. This filter was applied to measure the transmission of an optical band-pass filter and a fibered isolator, instead of a classical optical spectrum analyzer (OSA). Note that in most applications, the SC light is used as a broadband testing light with high power spectral density. In the case of STED microscopy, it is used to generate both the excitation and the STED wavelengths synchronously, significantly simplifying the experimental arrangement. The possibility of tuning these two wavelengths makes it possible to increase the range of fluorescein-type dyes for use in this application.

Compared to the SC light, the traditional white-light sources (WLSs) have some limitations in characterizing fiber optical components. Although halogen lamps and broadband LED-based light sources are versatile in a number of applications, the power spectral density of the former is limited by some low value, and the emission spectra of the latter are limited to a narrow range, which restricts their use for characterizing components at unconventional wavelengths [48–50]. In addition, the way they distribute their spectral power barely rises significantly above the detector noise level, which is a drawback for characterizing components in regions of high reflection or high loss, such as narrow-band (usually 20 pm to 1 nm) fiber Bragg gratings (FBGs) used as the selective reflectors of fiber-optic lasers and also in sensor applications [51–54]. Moreover, there are some applications in which it is necessary to capture ultrafast dynamics beyond conventional sources' time resolution.

In this work, we report the results of an experimental evaluation of a commercial supercontinuum laser (SCL) as a WLS for the characterization of passive optical components used in the implementation of fiber lasers and fiber optic sensors in the near-infrared range. The main premise of this work is that, under suitable alignment, the SCL can be used as a "universal" source of white light in an extensive wavelength range, from 1 to 2.1 μm, allowing one to obtain optical spectra, avoiding the use of multiple emission sources operating at specific wavelengths and, thus, significantly reducing the number of devices required for the characterization of the optical components. The fiber components under study were (i) fiber coupler (FC), (ii) wavelength-division multiplexers (WDMs), (iii) in-line fiber isolator (ISO), and (iv) home-made fiber Bragg gratings (FBGs).

We obtained, for all fiber components under study, the optical spectra using the SCL as a WLS and one of two OSAs of different wavelength ranges and compared the results with those obtained using a traditional WLS based on a halogen lamp and a 2 μm amplified spontaneous emission (ASE) light source. We applied this procedure to the characterization of WDM in an extensive range, from 1 to 2.4 μm, using direct focusing utilizing a condenser lens, and then transferred this knowledge to a number of components commonly used for assembling fiber lasers and fiber sensors, such as other varieties of WDMs, FCs, and ISO.

Then, we used this procedure to characterize FBGs in the narrow optical ranges. In the case of testing FBG at 2 μm, we included a simple monochromator (MC) in the experimental setup. The MC filtered the false diffraction orders of the OSA reflection grating observed in the 2 μm spectral range, which corresponds to the pump pulses' source operating in the 1 μm band for supercontinuum generation. In the case of FBG at 2 μm, the result achieved using SCL was compared with the one obtained using a commercial ASE source at 2 μm.

The main objective of this study is to demonstrate that a commercial SCL can be successfully used to characterize many types of passive fiber-optic components in the broad optical range. This opens up the possibility for a number of applications, such as the accurate interrogation of FBGs, the determination of fundamental loss levels in fibered optical isolators, the verification of transmission loss in fiber optical couplers and combiners, and the characterization of complex multi-component fiber devices.

2 Supercontinuum laser

The SCL used as a WLS is a commercial device that emits a collimated beam with a diameter of approximately 1 mm and a mean power of 1 W. According to the manufacturer data, its optical spectrum extends from 400 to 2,400 nm. Figure 1 shows the optical spectra measured in the spectral ranges (a) from 950 to 1,700 nm (OSA1, Table 1) and (b) from 1,200 to 2,200 nm (OSA2, Table 1). The spectral area near the wavelength of 1,060 nm (marked by P in plot (a)) corresponds to the ultra-short pulses that pump the nonlinear fiber of SCL, whereas the peak close to 2.12 µm (marked as FP in plot (b)) is a false spectral peak of the pump pulses seen at the double wavelength, which arises due diffraction of the spectral area P (plot (a)) to the second order of the reflective grating used as a spectral element of OSA2.

It is seen that the real spectral peak of pump pulses reaches the value of approximately −20 dB, and the false peak is smaller by a few dB. Note that the difference between the SC spectrum and the OSA dark noise is from about 54 to 46 dB (OSA1) and from 42 to 34 dB (OSA2), which allows one to measure the difference in transmission of about five orders in the former case and about three to four orders in the latter case. Note also that in the case of using OSA2 in the spectral range above 2 µm (on the right from the vertical dash line), one needs to use optical filtering of the spectrum related to the false spectrum peak. It should be noted that this problem was properly addressed in the experiments by implementing a low-cost MC, which operates as a simple selective filter avoiding the influence of the false peak without introducing significant complexity to the experimental arrangement.

Table 1: Equipment and materials used in the experiments

Equipment and fiber components used in the experiments
1. **Light sources**
• Supercontinuum laser, FYLA, model SCT-500.
• White Light Source, Yokogawa, model AQ4305.
• ASE source @ 2 µm, AdValue Photonics, model ASE AP-ASE-2100.
2. **Optical spectrum analyzers and monochromator**
• Optical Spectrum Analyzer 1 (OSA1): Yokogawa AQ6370D, 600–1,700 nm optical range.
• Optical Spectrum Analyzer 2 (OSA2): Yokogawa AQ6375, 1,200–2,400 nm optical range.
• Monochromator with operating range from 800 to 2,200 nm: Optometrics, model DMC1-06G.
3. **Fiber-optic components under test**
• WDM1: Commercial single-mode 1,135 nm/2,000 nm wavelength division multiplexer (WDM), Haphit.
• WDM2: Commercial single-mode 980/1550 nm WDM.
• FC: commercial single-mode fiber coupler, 50:50 at 1,320 nm.
• ISO: in-line fiber isolator, ThorLabs, model IO-H-1064B.
• FBG1: Home-made 85% fiber Bragg grating @ 1,134 nm.
• FBG2: Home-made 60% fiber Bragg grating @ 1,544 nm.
• FBG3: Home-made 99% fiber Bragg grating @ 2,076 nm.

We found that it is necessary to compare the SC spectrum with that of a traditional WLS based on a halogen lamp commonly used for testing fiber devices (Table 1); its spectrum is shown in Figure 1(a) by the green curve marked as WLS. It is seen that this spectrum is 20–35 dB below the SC spectrum; in the spectral range from 950 to 1,500 nm, it exceeds the OSA1 dark noise level by approximately 20 dB only. For the case of OSA2 (Figure 1(b)), the WLS spectrum is not shown because the noise level of the OSA2 is approximately 13 dB higher than that of the OSA1,

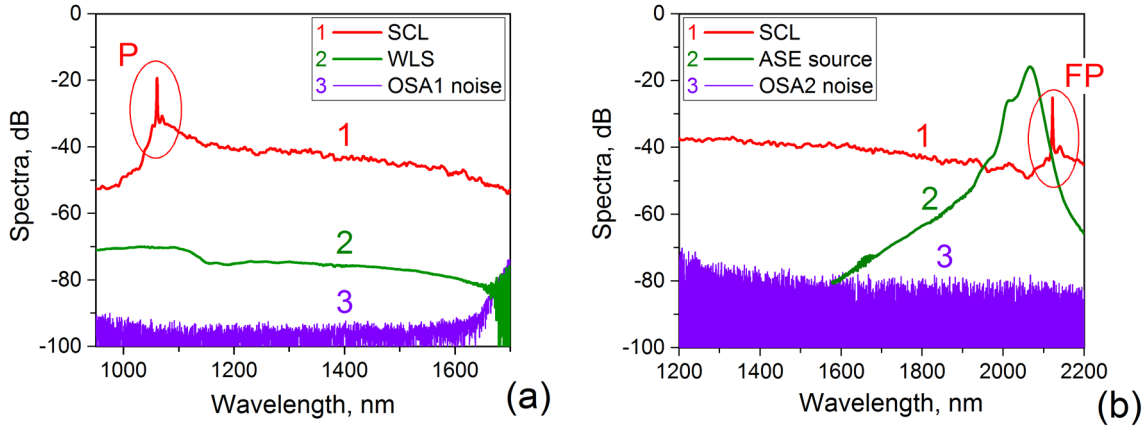

Figure 1: SCL optical spectra measured (a) with OSA1 (from 950 to 1,700 nm) and (b) with OSA2 (from 1,200 to 2,200 nm). The SCL spectra are demonstrated by the red curves 1. The green curve 2 demonstrates the WLS spectrum in plot (a) or the ASE source spectrum in plot (b). The OSAs' dark noise is shown in both plots by the violet curve 3 at the bottom. In both cases, the OSA resolution was 0.2 nm.

and the WLS spectrum is only slightly above the OSA2 noise. Therefore, it can be concluded that WLS cannot be used to characterize fiber optic devices with high accuracy, at least in the 2 µm range or when the OSA resolution is significantly higher (50 or 20 pm). In Figure 1(b), we also show, for comparison, the spectrum of the commercial source of ASE at 2 m, which was used in one of the experiments reported in this article.

As shown in Figure 1, the SCL-based characterization scheme provides higher power levels than other sources, reducing the dependence on the quality of spectrum analyzers. This allows it to be adapted for use with various types of OSA, even simpler and cheaper than those available in the laboratory for the current experiments.

3 Experimental setup

Table 1 lists the equipment used in the experimental realization of the techniques for the characterization of passive fiber-optic components and the components under test. Figure 2 presents images of some of the most important elements used in the experiments.

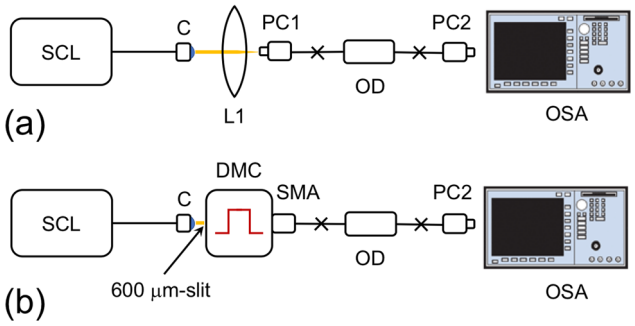

Figure 3: Experimental arrangements used for the characterization of (a) fiber optic components within the range below 2 µm and (b) FBGs in the 2 µm band.

Two experimental arrangements were implemented for the characterization of passive optical devices (OD), all in the near-infrared range commonly used in fiber lasers and sensors. Both of them are based on the SCL used as a test WLS.

The first arrangement, used in the wide optical range from 1 µm to just below 2 µm, does not involve optical filtering (monochromator), while the second one, used in the 2 µm range, does. The experimental setup corresponding to the first arrangement is shown in Figure 3(a). The

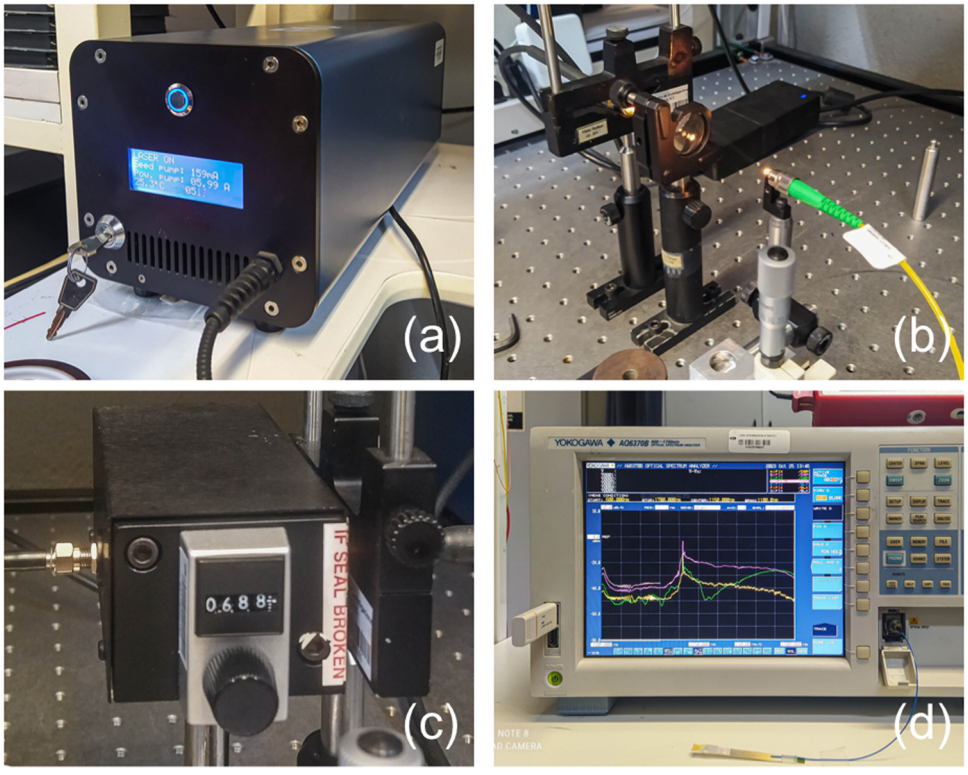

Figure 2: Photographs of the components and equipment used in the experimental setup: (a) the SCL, (b) the setup for alignment of the SCL output with the input fiber of the component under test, (c) the simple low-cost MC, and (d) OSA.

supercontinuum beam from the SCL collimated output was focused directly on the input of the single-mode (SM) plane fiber connector (PC1) of the device under characterization through a plano-convex lens (L) with a focal length of 5 cm. Due to simplicity, this arrangement is suitable for measuring the broad optical spectra that cover a large part of the OSA. This arrangement permits one to characterize also narrow-band fiber-optic components including FBGs in the spectrum range below 2 μm, using the OSAs' span of a few nanometers. PC2 is the plane optical connector of the SM patch cord used to connect the OD under study with the OSA.

To characterize FBGs with Bragg wavelength near 2 μm we used the experimental arrangement shown in Figure 3(b). In this case, the SCL beam passes first through the MC with a transmission window of about 10 nm and then enters the fiber-optic component under test. The peak wavelength of the transmission window can be tuned within the broad optical range according to the Bragg wavelength of the FBG under study. Another part of the arrangement is similar to that shown in Figure 3(a). As noted above, the importance of spectral filtering of the test beam relates to the fact that the SCL used as a WLS uses 1.06 μm short pulses to pump nonlinear fiber that, in turn, generates SC light. The OSA used for measuring optical spectra in the 2 μm range demonstrates the strong false spectral peak at the double wavelength of these pulses (at 2.12 μm, Figure 1(b)), which tends to dominate the components of the FBG spectrum. Therefore, the MC is the device that allows the measurement of transmission/reflection spectra of FBGs and other fiber optic passive components in the optical range of 2 μm. In this arrangement, an SM patch cord with an SMA fiber connector was used to deliver the narrow-band (filtered) SCL light to the OD under study. The 600 μm slit placed at the MC input limited the spectrum width of the SCL light at its output.

The entire set of experiments was performed under controlled laboratory conditions, with temperatures between 23 and 27°C and humidity of about 5%, which are within the safe operating limits of the low-power fiber devices under test. According to the manufacturers' specifications, the WDMs and couplers operate safely in the range of −45 to 80°C, and the isolator in the range of −5 to 50°C. For FBGs, maintaining the laboratory temperature at 25°C provided stable, consistent, and repeatable results in each measurement sequence. Otherwise, if the temperature is unstable, the grating Bragg wavelength varies with temperature with a slope of ~7–15 pm/°C, depending on the fiber type and the operating wavelength [55]. Humidity variations affect the Bragg wavelength of FBGs, written in a standard 125 μm silica fiber without special coating, to a lesser degree, but anyway, it is important to keep stable humidity of surrounding air [56] to prevent possible errors.

It should be noted that, generally, it is necessary to consider uncertainties that may affect the experiment results. In these cases, using fuzzy logic tools can be beneficial in measuring the degree of similarity between uncertain values [57]. Although this type of data processing is not discussed in this study, it opens the possibility of significantly improving data analysis when testing passive fiber optic components.

4 Results and discussion

4.1 Characterization of the 1,135 nm/2,050 nm WDM

In order to explore the possibility of using the SCL for the characterization of fiber-optic components, we selected a 1 × 2 extended-range 1,135 nm/2,000 nm wavelength division multiplexer (WDM1) for the first probe. This WDM can be used, for example, as a pump coupler for in-core pumping of Holmium-doped silica fiber laser or amplifier, when the pump power at approximately 1.13–1.15 μm is combined with the signal (laser) power at approximately 2 μm [58]. In this WDM, port 1 is the common port, port 2 is for 1,135 nm and port 3 is for 2,000 nm. Bare fiber adapters were placed at the ends of the device and the laser light was aligned using the arrangement shown in Figure 1(a). The measurement was performed using the SCL as a WLS and two OSAs, OSA1 and OSA2; the result of this experiment is shown in Figure 4.

From Figure 4, one can see that the optical loss between ports P1 and P2 at the "pump wavelength" (1,135 nm, plot (a)) is much less than the loss at the "signal wavelength" (near 2 μm, plot (b)), while the loss between P1 and P3 shows the opposite trend. It should be noted that the spectrum above approximately 1,950 nm (see plot (b)) is influenced by the false spectral peak of the pump pulses of the SCL (the spectral area A).

By combining the optical spectra measured from the WDM1 output, we obtained its normalized transmission spectra, which are shown in Figure 5(a). In this figure, similar to Figure 4, the transmission curve marked by 1 corresponds to the optical path from port 1 to port 2 and one marked by 2 for the path from port 1 to port 3. From this figure, one can see that the WDM1 is characterized by the relatively plain transmission spectrum in the optical range of 1,050–1,250 nm and by the narrow optical spectrum in the range near 2,000 nm with the peak transmission/loss at 1,950 nm. It is also seen that in area A (above

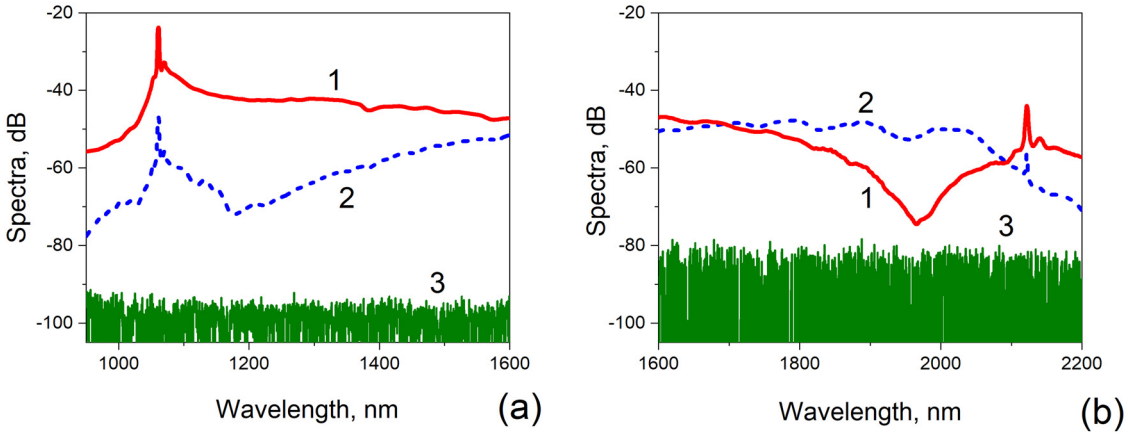

Figure 4: Spectra recorded at the different combinations of WDM ports measured with (a) OSA1 and (b) OSA2. The spectra corresponding to the SCL light passed from port P1 to P2 and from P1 to P3 are shown by the red solid (curve 1) and the blue dash (curve 2) lines, respectively. The OSAs' dark noise spectra are shown by the green lines 3.

2 µm) the spectra are affected by the false spectral peak centered at 2.12 µm. Note that the discussed spectra were obtained after dividing the linear transmission spectra by their sum.

To correct the discussed spectra, measured with OSA2 and SCL as a WLS, we used, instead of the latter, the ASE source that operates in the narrow optical range near 2 µm; its spectrum is shown in Figure 1(b). The new transmission spectra measured in the 2 µm range were combined with those measured using SCL and OSA1 below 1,600 nm; the result is shown in Figure 5(b). From this figure, one can see that these transmission spectra are characterized by smooth spectral variations above 2 m instead of jumps shown in Figure 5(a). Moreover, the corrected transmission peaks are broader and symmetrical relative to the peak wavelength at 1,950 nm. We believe that similar spectra could be obtained using SCL and the OSA2 in combination with a long-pass optical filter with a cutoff wavelength ranging from 1,200 to 1,600 nm.

4.2 Characterization of some frequently used FCs

Using the arrangement shown in Figure 1(a) and the OSA1, we characterized two SM fiber components commonly used in fiber lasers, amplifiers, and sensors. One of them was a 1 × 2 broadband 980/1550 WDM (WDM2), and another one was a 2 × 2 SM 50:50 FC at 1,350 nm. Transmission spectra of these components are presented in Figure 6 in linear scale: plot (a) shows transmission of the WDM2

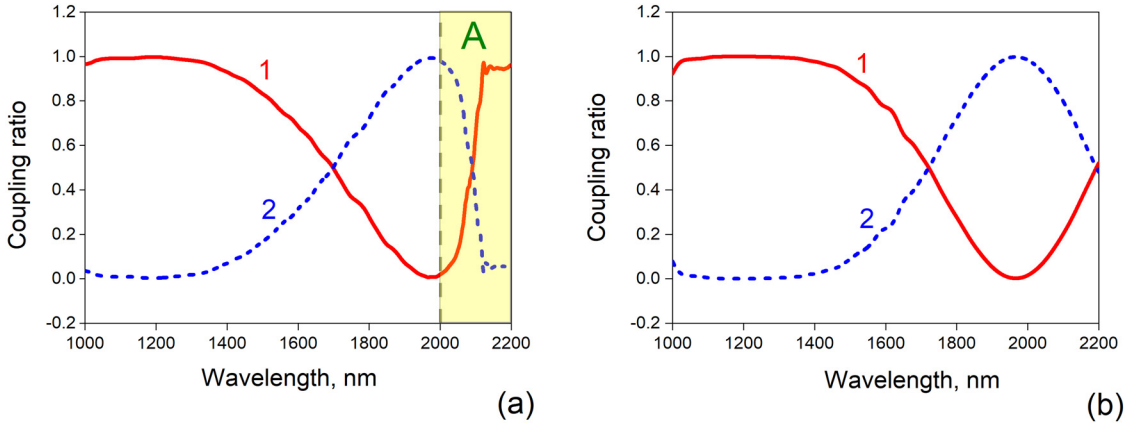

Figure 5: The normalized transmission spectra of the 1,135/2,000 nm WDM1 shown in the linear scale. The spectra are measured using (a) SCL only and (b) SCL (below 1,600 nm) and ASE source (above 1,600 nm) as WLSs. In both plots, the solid curve 1 and the dashed curve 2 correspond to WDM1's transmission from port 1 to port 2 and from port 1 to port 3, respectively.

whereas plot (b) demonstrates transmissions of the FC. In the case of WDM2, the common port number is 1, the number of the pump port (980 nm) is 2, and the number of the signal port (1,550 nm) is 3. In the case of the 50:50 FC, ports 1 and 2 are on one side of the device, whereas ports 3 and 4 are on the other side.

Figure 6 shows the transmission spectra of (a) the WDM2 and (b) the FC, both in the optical range above 950 nm (SM regime) and below 1,700 nm (the OSA1's limit). It is seen that the obtained transmission spectra of each fiber device are characterized by the wide plain area near 1 μm and by the peak of transmission/loss around 1,550 nm. The ratio of 50:50 between the transmissions from port 1 to ports 3 and 4 of FC is observed at 1,350 nm, which corresponds to the design parameters of the multiplexer. In the case of the WDM2, the wavelength at which the same ratio is reached is slightly shifted to the right (1,374 nm). But anyway, in spite of WDM2 and FC being designed for different tasks, their characteristics are quite similar.

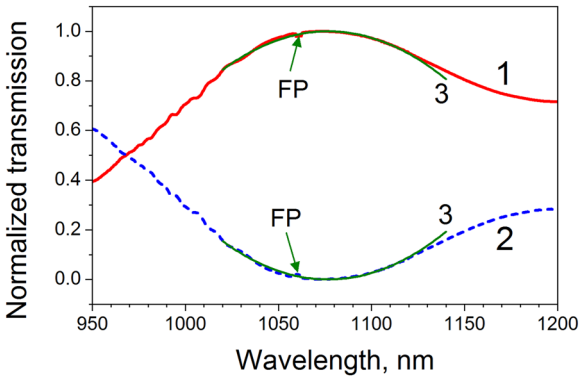

Figure 7: Transmission curves obtained for the in-line fiber isolator. Curves 1 and 2 demonstrate the forward and the backward light transmissions. The arrows FP show the small peaks at 1,060 nm arising due to the spectral peak of SCL partially compensated at this wavelength (Figure 1).

Both experimental curves shown in this plot are fitted with high precision near the peak wavelength by the parabolic functions (see olive curves marked as 3).

4.3 Characterization of in-line fiber isolator

The next device characterized using SCL was an in-line fiber polarization-independent isolator commonly used in low-power ytterbium fiber lasers and amplifiers. This device has the maximum transmission to the forward propagation and the maximum loss to the backward propagation of light at the design wavelength, see Figure 7, in which the light transmissions normalized to the minimum isolator loss (about 2.5 dB) for the forward light propagation are shown. From this figure, one can see that the minimum loss for the forward propagation and the highest backward loss are observed at approximately 1,070 nm.

4.4 Characterization of FBGs

An FBG consists of a periodic variation of the refractive index in the core of an optical fiber, to produce the reflection of a specific wavelength without affecting the rest of the spectrum [59–61]. We measured the transmission spectra of three FBGs with the Bragg wavelengths at different parts of the IR spectrum, from 1 μm to above 2 μm. Two FBGs with spectra in the range OSA1 (<1,700 nm) were tested: the first one (FBG1), with reflection of 85%, was centered at ~1,134 nm, while the second one (FBG2), with reflection of 70%, was centered at ~1,544 nm. The

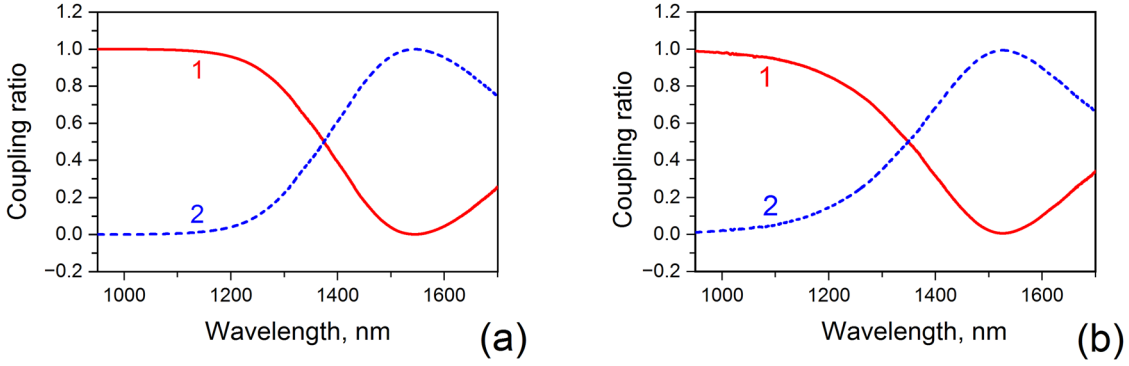

Figure 6: Transmission spectra obtained for (a) WDM2 and (b) FC. In both plots, the red solid line 1 and the blue dashed line 2 show transmissions from the common plot 1 to (a) plots 2 and 3 and (b) to plots 3 and 4, respectively. In the case of FC, the transmission spectra from port 2 to ports 3 and 4 are not shown since they are very similar to the presented ones.

transmission spectra were obtained in both cases using arrangements without the MC, as shown in Figure 1(a). In the case of FBG3 with the Bragg wavelength at 2071.7 nm, the MC was used as a spectrally selective device filtering the false diffraction orders of the OSA2's diffraction grating out.

Figure 8(a1) and (b1) shows the transmission spectra of FBG1 and FBG2 measured using the OSA1 with the resolution of 20 pm. The spectra were obtained after subtraction of the logarithmic (in dB) FBGs' spectra registered with and without gratings after recalculating the results to the linear scale. Figure 8(a1) demonstrates the transmission spectrum in the broader wavelength range that permits one to observe small peaks corresponding to the light energy transfer from the propagation mode LP_{01} to the co-propagating cladding modes LP_{0n} of the fiber (see the area A marked with the orange ellipse) [59], which are not presented in the reflection spectrum of the grating. This observation confirms that an SCL is a broadband WLS with sufficiently high spectral density, permitting one to detect the details of the FBGs' spectra.

Figure 8(a2) and (b2) show the reflection spectra of the gratings computed from the correspondent transmission curves; see the blue solid lines 1. From these spectra, one may obtain the FBGs' reflections: 81 and 64% for FBG1 and FBG2, respectively. The spectrum widths measured as the full width at half of the maximum (FWHM) are 90 pm for FBG1 and 70 pm for FBG2. It is seen that the reflection spectrum of FBG1 consists of two peaks that differ by an order of magnitude; the weak one can be related to an incontrollable chirp induced during FBG writing. The red dashed lines fit the reflection spectra: the FBG1 spectrum is fit by the pseudo-Voigt peak function (a linear combination of the Gaussian and the Lorentzian peaks) without considering sub-peak 2 (see plot (a2)), whereas the FBG2 spectrum is fit by the function describing the reflection spectrum of the uniform FBG of ~1.5 cm length [61]. Note that in the former case, this kind of fit can be used for FBG with some grade of unwanted chirp and apodization, and in the latter case, FBG is approximately ideal with some imperfections below 4% of reflection occurring due to limited OSA resolution, possible week light interference, and small grating imperfections.

The spectra of FBG3, centered at 2071.8 nm, were measured using the MC placed between the SCL and the input of the fiber with the grating (Figure 3(b)), which permitted one to eliminate the false spectral peak registered by 2-μm OSA shown in Figure 1(b).

As was already discussed above, for measuring FBG spectra in the range near 2 μm, one should apply the experimental arrangement shown in Figure 3(b). This arrangement permits filtering out the false spectral peak of SCL light arising at this range of wavelengths in the traces collected by OSA2 (Figure 1(b)). Figure 9 shows (a) the normalized spectra of the light sources used for the FBG3 testing and

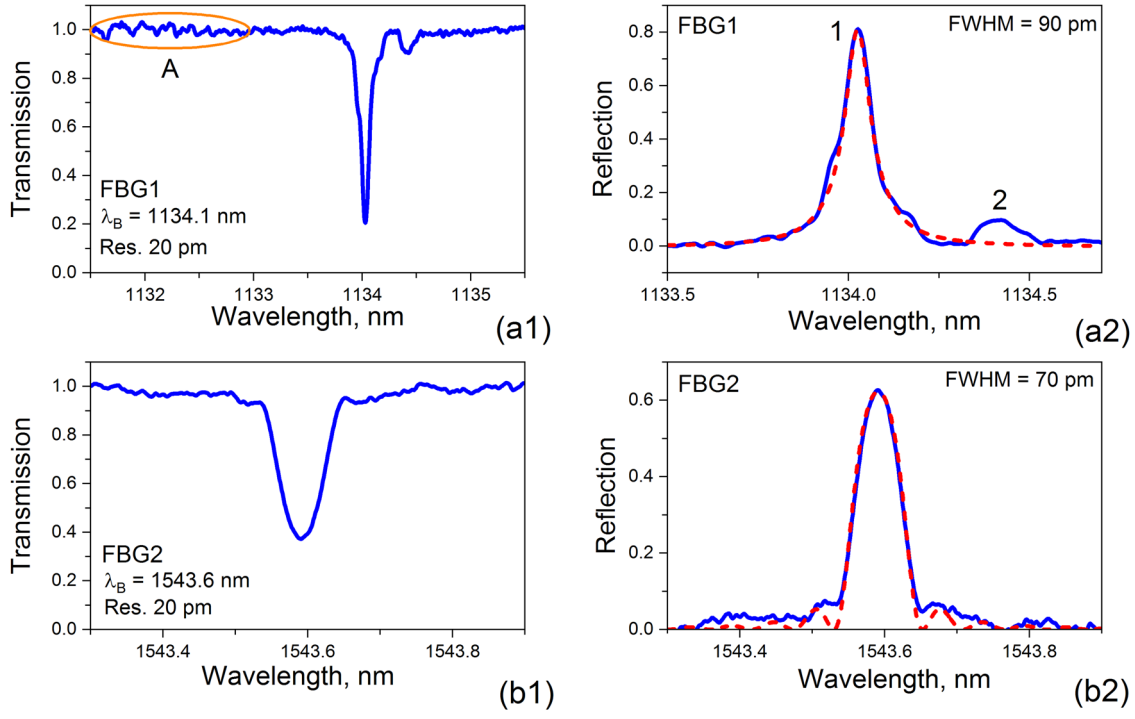

Figure 8: The linear transmission and reflection of FBG1, plots (a1) and (a2), and FBG2, plots (b1) and (b2).

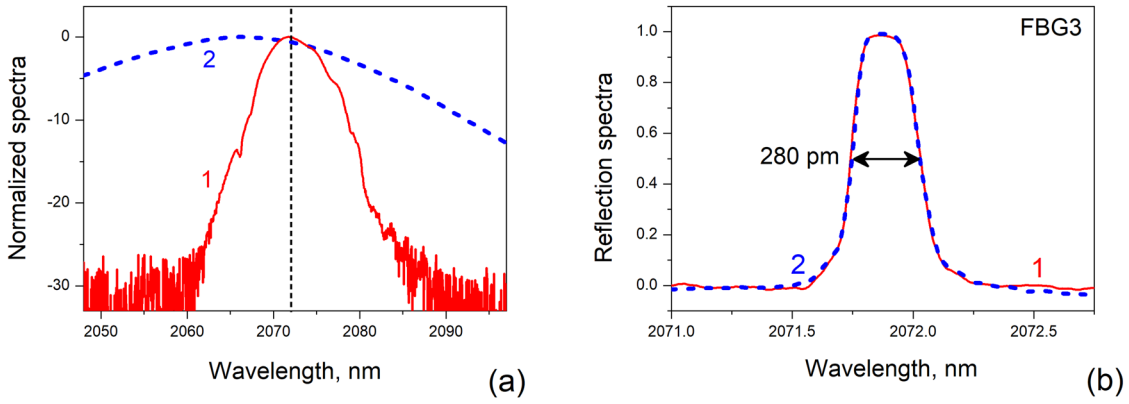

Figure 9: (a) Normalized spectra of the broad-band light sources used for characterization of FBG3 measured in the 50-nm range. The red solid line 1 and the blue dashed line 2 show the spectrum of the SCL light measured from the MC output and that of the ASE source, respectively. The vertical dash line indicates the Bragg wavelength of FBG3. (b) FBG3 reflection spectra obtained using SCL light (the red solid line 1) and ASE source (the blue dashed line 2).

(b) the results of this testing. Note that FBG3 was used as the rear reflector of the holmium-doped fiber laser cavity, which is characterized by high reflection at the Bragg wavelength (about 100%).

As is seen from Figures 1(b) and 9(a), both broad-band light sources used for FBG3 testing, demonstrate a signal-to-noise ratio of about 60 dB for the ASE source and 25 dB for the filtered SCL source, which is enough for the characterization of FBGs with the peak reflection as higher as 99.7% or slightly more. The reflection spectra of FBG3 obtained using these light sources are shown in Figure 9(b). In this figure, the spectra measured using the filtered SCL and ASE source are shown in curve 1 and curve 2, respectively. The spectra are very similar to each other; their width measured as FWHM is 280 pm. The maximum of FBG3 reflection (R) measured with SCL light is 98.6%, whereas that measured with ASE source is 99.2%, which demonstrates the difference in reflection of about half of a percent. This result confirms the validity of using a standard SC source for testing FBGs.

5 Conclusions

In the present work, we demonstrated that an SCL can be used as a versatile WLS for characterizing passive fiber optic components in the infrared optical range. We also showed that SCL can be successfully applied for testing fiber components of different types, such as FCs, WDMs, and fiber isolators, in the broad optical range. We demonstrated that SCL can also be applied for narrow-band spectral measurements, for instance, for testing FBGs.

Since the commercial OSA used in the present study demonstrates false spectral peaks in the optical range from 2.0 to 2.2 μm, which correspond to the double wavelength of ultra-short optical pulses that pump a nonlinear fiber of SCL, optical filtering is needed to suppress these unwanted spectral components for reliable characterization of fiber components in this range. For this aim, we used an inexpensive commercial MC, which allowed us to test fiber optic components with high precision, including FBGs, in the 2 μm range.

The results of testing fiber components in the 2 μm range obtained using SCL and a low-cost MC as a tunable optical filter were confirmed by experiments with a commercial 2 μm light source based on ASE, which covers the optical range from 1,900 to 2,100 nm, whereas that acquired at the wavelengths below 2 μm, were verified applying halogen-lamp-based WLS. Both arrangements demonstrated very similar results.

The presented research is of particular interest in the development of fiber lasers and fiber sensors operating in the wavelength range covered by the broadband SCL utilized as a control light source for testing passive fiber optic components used in these devices.

Funding information: This research was funded in part by the CONAHCyT, Mexico, project number CF-2023-I-2431, the Ministerio de Ciencia e Innovación/Agencia Estatal de Investigación, Spain, grant number MCIN/AEI/10.13039/501100011033, co-funded by the European Union "ERDF A way of making Europe", under grant PDI2019-104276RB-I00, and by the Generalitat Valenciana, Spain (CIPROM/2022/30). P Muniz-Cánovas acknowledges financial support from CONAHCyT, Mexico, as part of the "Postdoctoral Fellowships for Mexico 2022(1)", CVU 700792.

Author contributions: Pablo Muniz-Cánovas: investigation, data curation, writing – original draft. Yuri Barmenkov: funding acquisition, investigation, writing – review and editing, supervision, project administration. Ambar A. Reséndiz-Córdova: investigation. Vicente Aboites: writing – investigation, review and editing, José-Luis Cruz: formal analysis, investigation. Miguel V. Andrés: funding acquisition, review and editing. All authors have accepted responsibility for the entire content of this manuscript and approved its submission.

Conflict of interest: The authors state no conflict of interest.

Data availability statement: The datasets generated and/or analyzed during the current study are available from the corresponding author on reasonable request.

References

[1] Maker PD, Terhune RW, Savage CM. Intensity-dependent changes in the refractive index of liquids. Phys Rev Lett. 1964;16:832.

[2] Bloembergen N, Lallemand P. Complex intensity-dependent index of refraction, frequency broadening of stimulated Raman lines, and stimulated Rayleigh scattering. Phys Rev Lett. 1966;16:81–4.

[3] Alfano RR, Gersten JI, Zawadzkas GA, Tzoar N. Self-phase-modulation near electronic resonances of a crystal. Phys Rev A. 1974;10:698–708.

[4] Alfano RR, Wang QZ, Jimbo T, Ho PP, Bhargava RN, Fitzpatrick BJ. Induced spectral broadening about a second harmonic generated by an intense primary ultrashort laser pulse in ZnSe crystals. Phys Rev A. 1987;35(1):459.

[5] Alfano RR, Ho PP, Fleury PA, Guggenheim HJ. Nonlinear optical effects in antiferromagnetic KniF3. Opt Commun. 1976;19(2):261–4.

[6] Bloembergen N, Lallemand P, Pine A. 6A2 – The influence of self-focusing on the stimulated Brillouin, Raman, and Rayleigh effects. IEEE J Quantum Electron. 1966;2(8):246–8.

[7] Geng W, Fang Y, Wang Y, Bao C, Liu W, Pan Z, et al. Nonlinear photonics on integrated platforms. Nanophotonics. 2024;13(18):3253–78.

[8] Agrawal GP, Potasek MJ. Nonlinear pulse distortion in single-mode optical fibers at the zero-dispersion wavelength. Phys Rev A. 1986;33(3):1765.

[9] Akhmediev N, Karlsson M. Cherenkov radiation emitted by solitons in optical fibers. Phys Rev A. 1995;51(3):2602.

[10] Reddy PH, Kir'yanov AV, Dhar A, Das S, Dutta D, Pal M, et al. Fabrication of ultra-high numerical aperture GeO_2-doped fiber and its use for broadband supercontinuum generation. Appl Opt. 2017;56:9315–23.

[11] Momgaudis B, Marčiulionytė V, Jukna V, Tamošauskas G, Barkauskas M, Dubietis A. Supercontinuum generation in bulk solid-state material with bursts of femtosecond laser pulses. Sci Rep. 2024;14:7055.

[12] Birks TA, Wadsworth WJ, Russell PS. Supercontinuum generation in tapered fibers. Opt Lett. 2000;25(19):1415.

[13] Wadsworth WJ, Ortigosa-Blanch A, Knight JC, Birks TA, Martin Man T-P, Russell PS. Supercontinuum generation in photonic crystal fibers and optical fiber tapers: a novel light source. J Opt Soc Am B. 2002;19(9):2148.

[14] Zhang H, Zu J, Liu X, Chen J, Xu H. High power all-fiber supercontinuum system based on graded-index multimode fibers. Appl Sci. 2022;12:5564.

[15] Husakou AV, Herrmann J. Supercontinuum generation of higher-order solitons by fission in photonic crystal fibers. Phys Rev Lett. 2001;87(20):203901.

[16] Kiroriwal M, Singal P. Design and analysis of highly nonlinear, low dispersion AlGaAs-based photonic crystal fiber. J Opt Commun. 2023;44(1):s589–95.

[17] García S, Ureña M, Gasulla I. Dispersion-diversity multicore fiber signal processing. ACS Photonics. 2022;9(8):2850–9.

[18] Carlson DR, Hickstein DD, Lind A, Olson JB, Fox RW, Brown RC, et al. Photonic-chip supercontinuum with tailored spectra for counting optical frequencies. Phys Rev Appl. 2017;8(1):014027.

[19] Watt RS, Kaminski CF, Hult J. Generation of supercontinuum radiation in conventional single-mode fibre and its application to broadband absorption spectroscopy. Appl Phys B. 2008;90:47–53.

[20] Kano H, Hamaguchi H. Characterization of a supercontinuum generated from a photonic crystal fiber and its application to coherent Raman spectroscopy. Opt Lett. 2003;28:2360–2.

[21] Hickstein DD, Kerber GC, Carlson DR, Chang L, Westly D, Srinivasan K, et al. Quasi-phase-matched supercontinuum generation in photonic waveguides. Phys Rev Lett. 2018;120(5):053903.

[22] Schenkel B, Paschotta R, Keller U. Pulse compression with supercontinuum generation in microstructure fibers. J Opt Soc Am B. 2005;22:687–93.

[23] Gladyshev A, Yatsenko Y, Kolyadin A, Bufetov I. Visible to mid-infrared supercontinuum initiated by stimulated Raman scattering of 1.03 μm ultrashort pulses in a gas-filled silica fiber. Photonics. 2022;9:997.

[24] Kaminski CF, Watt RS, Elder AD, Frank JH, Hult J. Supercontinuum radiation for applications in chemical sensing and microscopy. Appl Phys B. 2008;92:367–78.

[25] Kim S, Jeong T, Park J, Ciappina MF, Kim S. Recent advances in ultrafast plasmonics: from strong field physics to ultraprecision spectroscopy. Nanophotonics. 2022;11(11):2393–431.

[26] Poudel C, Kaminski CF. Supercontinuum radiation in fluorescence microscopy and biomedical imaging applications. J Opt Soc Am B. 2019;36:A139–53.

[27] Wildanger D, Rittweger E, Kastrup L, Hell SW. STED microscopy with a supercontinuum laser source. Opt Express. 2008;16(13):9614–21.

[28] Glubokov DA, Sychev VV, Vitukhnovsky AG, Korol'kov AE. Photonic crystal fibre-based light source for STED lithography. Quant Electron. 2013;43(6):588–90.

[29] Rao DS, Jensen M, Grüner-Nielsen L, Olsen JT, Heiduschka P, Kemper B, et al. Shot-noise limited, supercontinuum-based optical coherence tomography. Light Sci Appl. 2021;10:133.

[30] Moon S, Kim DY. Ultra-high-speed optical coherence tomography with a stretched pulse supercontinuum source. Opt Express. 2006;14(24):11575–84.

[31] Humbert G, Wadsworth WJ, Leon-Saval SG, Knight JC, Birks TA, Russell PS, et al. Supercontinuum generation system for optical coherence tomography based on tapered photonic crystal fibre. Opt Express. 2006;14:1596–603.

[32] Yin S, Ruffin P, Brantley C, Edwards E, Luo C. Mid-IR supercontinuum generation and applications: a review. Proc SPIE. 2014;9200:130–41.

[33] Sang X, Yu C, Ma J, Xin X, Wang K, Zhang Q. Low noise supercontinuum generated in the photonic crystal fiber for microwave photonic applications. Optoelectron Adv Mater – Rapid Comm. 2009;3(2):85–8.
[34] Heidt AM, Hartung A, Bartelt H. Generation of ultrashort and coherent supercontinuum light pulses in all-normal dispersion fibers. In: Aftano RR, editor. The supercontinuum laser source. New York: Springer; 2016.
[35] Melchert O, Brée C, Tajalli A, Pape A, Arkhipov R, Williams S, et al. All-optical supercontinuum switching. Commun Phys. 2020;3:146.
[36] Ray P, Salido-Monzú D, Camenzind SL, Wieser A. Supercontinuum-based hyperspectral LiDAR for precision laser scanning. Opt Express. 2023;31:33486–99.
[37] Saleh A, Aalto A, Ryczkowski P, Genty G, Toivonen J. Short-range supercontinuum-based lidar for temperature profiling. Opt Lett. 2019;44:4223–6.
[38] Xu T, Ma X, Li Q, Lu Y. Application of low-altitude wind shear recognition algorithm and laser wind radar in aviation meteorological services. Open Phys. 2023;21(1):20230154.
[39] Dennis T, Yasanayake C, Gerke T, Payne A, Eng L, Fischer B, et al. A programmable solar simulator for realistic seasonal, diurnal, and air-mass testing of multi-junction concentrator photovoltaics. IEEE 43rd Photovoltaic Specialists Conference (PVSC). Portland, U; 2016. p. 2327–32.
[40] Kudlinski A, Barviau B, Leray A, Spriet C, Héliot L, Mussot A. Control of pulse-to-pulse fluctuations in visible supercontinuum. Opt Express. 2010;18:27445–54.
[41] Shan B, Ghimire S, Chang Z. Generation of the attosecond extreme ultraviolet supercontinuum by a polarization gating. J Mod Opt. 2005;52(2–3):277–83.
[42] Hammond T, Monchocé S, Zhang C, Vampa G, Klung D, Yu, et al. Integrating solids and gases for attosecond pulse generation. Nat Photonics. 2017;11:594–9.
[43] Kim KY, Taylor AJ, Glownia JH, Rodriguez G. Coherent control of terahertz supercontinuum generation in ultrafast laser–gas interactions. Nat Photonics. 2008;2:605–9.
[44] Ruehl A, Martin MJ, Cossel KC, Chen L, McKay H, Thomas B, et al. Ultrabroadband coherent supercontinuum frequency comb. Phys Rev A. 2011;84:011806(R).
[45] Nicholson JW, Yan MF. Cross-coherence measurements of supercontinua generated in highly-nonlinear, dispersion shifted fiber at 1550 nm. Opt Express. 2004;12:679–88.
[46] Narukawa Y, Ichikawa M, Sanga D, Sano M, Mukai T. White light emitting diodes with super-high luminous efficacy. J Phys D: Appl Phys. 2010;43:354002.
[47] Lehtonen M, Genty G, Ludvigsen H. Absorption and transmission spectral measurement of fiber-optic components using supercontinuum radiation. Appl Phys B. 2005;81:231–4.
[48] Castagna N, Jacques Morel J. Fibre-coupled tunable source based on a supercontinuum laser for the spectral characterization of fibre optics components and systems. Metrologia. 2022;59:035005.
[49] Jia Z, Yuan C, Liu Y, Wang X, Sun P, Wang L, et al. Strategies to approach high performance in Cr3+ -doped phosphors for high-power NIR-LED light sources. Light Sci Appl. 2020;9:86.
[50] Xiao Z, Qin S, Guo X, Xu X, Anaerguli W, Jiang W, et al. Efficient and broadband near-infrared emission of Cr3 + -doped glass-ceramics for near-infrared light sources applications. J Lumin. 2022;247:118907.
[51] Sano Y, Yoshino T. Effect of light source spectral modulation on wavelength interrogation in fiber Bragg grating sensors and its reduction. IEEE Sens J. 2003;3(1):44–9.
[52] Karapanagiotis C, Schukar M, Krebber K. Distributed fiber optic sensors for structural health monitoring of composite pressure vessels. tm – Tech Mess. 2024;91(3–4):168–79.
[53] Lee JY, Kim DY. Versatile chromatic dispersion measurement of a single mode fiber using spectral white light interferometry. Opt Express. 2006;14:11608–15.
[54] Zhang X, Tao Z, Yang L. Temperature detection technology of power equipment based on Fiber Bragg Grating. Open Phys. 2018;16(1):663–7.
[55] Byoungho L. Review of the present status of optical fiber sensors. Opt Fiber Technol. 2003;9:57–79.
[56] Aris AM, Irawati N, Rahman HA, Harun SW, Ahad IZM. Fiber Bragg grating sensor for humidity measurement. Proc. IEEE International Conference on System Engineering and Technology. 2015. p. 55–9.
[57] Versaci M, Angiulli G, di Barba P, Morabito FC. Joint use of eddy current imaging and fuzzy similarities to assess the integrity of steel plates. Open Phys. 2020;18(1):230–40.
[58] Kir'yanov AV, Barmenkov YO, Villegas-Garcia IL, Cruz JL, Andres MV. Highly efficient holmium-doped all-fiber ~2.07-μm laser pumped by Ytterbium-doped fiber laser at ~1.13 μm. IEEE J Sel Top Quantum Electron. 2018;24(5):0903108.
[59] Kalli K, Othonos A. Fiber Bragg gratings: fundamentals and applications in telecommunications and sensing. Boston: Artech House; 1999. Chap. 5.
[60] Hill KO, Meltz G. Fiber Bragg grating technology fundamentals and overview. J Light Technol. 1997;15(8):1263–76.
[61] Kashyap R. Fiber Bragg gratings. San Diego: Academic Press; 1999. Chap. 4.